

# Anisotropic Edge-based Balloon Eikonal Active Contours

Da Chen and Laurent D. Cohen

CEREMADE, CNRS,  
University Paris Dauphine, PSL Research University,  
UMR 7534, 75016 PARIS, FRANCE

**Abstract.** In this paper, we propose a new edge-based active contour model for image segmentation and curve evolution by an asymmetric Finsler metric and the corresponding minimal paths. We consider the edge anisotropy information and the balloon force term to build a Finsler metric comprising of a symmetric quartic term and an asymmetric linear term. Unlike the traditional geodesic active contour model where the curve evolution is carried out by the level set framework, we search for a more robust optimal curve by solving an Eikonal partial differential equation (PDE) associated to the Finsler metrics. Moreover, we present an interactive way for geodesics extraction and closed contour evolution. Compared to the level set-based geodesic active contour model, our model is more robust to spurious edges, and also more efficient in numerical solution.

## 1 Introduction

Active contours model or the snakes model [1] was proposed by Kass *et al.* for boundary detection. The basic idea is to extract a sequence of time-dependent curves to minimize the curve-based energy where the limit of these curves denotes the boundary of an object. The snakes energy involves a potential function  $P$  such that  $E_{\text{snake}}(\gamma) = \int_0^1 (\eta_1 \|\gamma'(v)\|^2 + \eta_2 \|\gamma''\|^2 + P(\gamma(v))) dv$ , where  $\eta_1$  and  $\eta_2$  are two constants. A curve  $\gamma \in H^2([0, 1], \Omega)$  lies at an open domain  $\Omega \subset \mathbb{R}^2$  with  $H^2$  is a Sobolev space. The terms  $\|\gamma'\|$  and  $\|\gamma''\|$  are respective the first- and second-order derivatives of the path  $\gamma$ . In the past decades, a series of approaches have been devoted to overcome the drawbacks of the snakes model [1] such as the initialization sensitivity and the dependence of the parameterization.

The geodesic active contours (GAC) model [2, 3] reformulated the snakes energy  $E_{\text{snake}}$  and removed the second-order derivative  $\|\gamma''\|$  from  $E_{\text{snake}}$ . The GAC model leads to important theoretical results. However, in its basic formulation, the geodesic metric is actually an isotropic Riemannian metric which cannot take into account the curve orientation. In [4, 5], the authors extended the isotropic metric to the anisotropic case and the Finslerian case. The curve evolution is originally carried out based on the level set framework [6] and the Euler-Lagrange equation. Such a curve evolutionary strategy costs expensive computation time

and known to be sensitive to noise and spurious edges due to the numerous undesired local minimums. Cohen and Kimmel [7] proposed an efficiently minimal path model, which can be naturally used for open curve detection. For object segmentation, more efforts [8–10] have been devoted to for closed contours detection which are used to delineate object boundaries.

In this paper, we propose a new curve evolution scheme based on the Eikonal interpretation framework of a general regional active contour energy [10]. The main contribution lies at the construction of a Finsler metric induced from the balloon force [11] and the anisotropic edge information. In contrast to [10], our method mainly depends on the anisotropic edge saliency information and balloon force, which is insensitive to gray levels inhomogeneities.

## 2 Background on Minimal path and Eikonal PDE

Let  $\mathfrak{S}([0, 1], \Omega)$  be the collection of all Lipschitz continuous curves  $\gamma : [0, 1] \rightarrow \Omega$ . We denote by  $S_2^+$  the collection of  $2 \times 2$  symmetric positive definite matrices. A norm  $\|\mathbf{u}\|_M$  is defined by  $\sqrt{\langle \mathbf{u}, M\mathbf{u} \rangle}$ , where  $M \in S_2^+$ .

Cohen and Kimmel [7] proposed an Eikonal PDE-based method to globally minimize the following geodesic energy  $\mathcal{L}_{\text{Iso}}(\gamma) := \int_0^1 (\mathcal{P}(\gamma(t)) + \epsilon) \|\gamma'(t)\| dt$  with  $\epsilon > 0$  a constant used for minimal geodesic regularization. The geodesic distance map  $\mathcal{U}$  associated to a source  $\mathbf{s}$  is defined as  $\mathcal{U}_{\mathbf{s}}(\mathbf{x}) := \min\{\mathcal{L}_{\text{Iso}}(\gamma); \gamma \in \mathfrak{S}([0, 1], \Omega)\}$ , which is the viscosity solution to the isotropic Eikonal PDE [7]

$$\|\nabla \mathcal{U}(\mathbf{x})\| = \mathcal{P}(\mathbf{x}) + \epsilon, \quad \forall \mathbf{x} \in \Omega \setminus \{\mathbf{s}\}, \quad \text{and} \quad \mathcal{U}(\mathbf{s}) = 0. \quad (1)$$

A general Finsler metric  $\mathcal{F} : \Omega \times \mathbb{R}^2 \rightarrow \mathbb{R}^+$  is a positive, 1-homogeneous, and potentially asymmetric function [4, 12], based on which the curve length associated to the Finsler metric  $\mathcal{F}$  is defined by  $\mathcal{L}_{\mathcal{F}}(\gamma) := \int_0^1 \mathcal{F}(\gamma(t), \gamma'(t)) dt$ . The Finsler Eikonal PDE [12–15] associated to  $\mathcal{L}_{\mathcal{F}}$  can be expressed by

$$\sup_{\|\mathbf{v}\|=1} \frac{\langle \nabla \mathcal{U}(\mathbf{x}), \mathbf{v} \rangle}{\mathcal{F}(\mathbf{x}, \mathbf{v})} = 1, \quad \forall \mathbf{x} \in \Omega \setminus \{\mathbf{s}\}, \quad \forall \mathbf{u} \in \mathbb{R}^2, \quad \text{and} \quad \mathcal{U}(\mathbf{s}) = 0. \quad (2)$$

We consider the Randers metric [16], a special Finsler metric with the form of

$$\mathcal{F}(\mathbf{x}, \mathbf{u}) = \|\mathbf{u}\|_{\mathcal{M}(\mathbf{x})} + \langle \boldsymbol{\omega}(\mathbf{x}), \mathbf{u} \rangle, \quad \forall \mathbf{x} \in \Omega, \quad \forall \mathbf{u} \in \mathbb{R}^2, \quad (3)$$

where  $\mathcal{M} : \Omega \rightarrow S_2^+$  is a positive symmetric definite tensor field and  $\boldsymbol{\omega} : \Omega \rightarrow \mathbb{R}^2$  is a vector field. The tensor field  $\mathcal{M}$  and the vector field  $\boldsymbol{\omega}$  should satisfy

$$\langle \boldsymbol{\omega}(\mathbf{x}), \mathcal{M}^{-1}(\mathbf{x}) \boldsymbol{\omega}(\mathbf{x}) \rangle < 1, \quad \forall \mathbf{x} \in \Omega, \quad (4)$$

to ensure the positivity of  $\mathcal{F}$  [13, 16].

### 3 Edge-based Balloon Eikonal Active Contours

**Geodesic interpretation of an edge-based balloon energy.** Let  $\chi_B$  be the characteristic function of a region  $B \subset \Omega$ . The balloon force [11] was designed as external force for active contours by minimizing the region-based term [17]

$$E_{\text{balloon}}(\chi_B) = \int_{\Omega} \chi_B(\mathbf{x}) d\mathbf{x} = \int_B d\mathbf{x}, \quad (5)$$

where  $B \subset \mathbb{R}^2$  is the interior region of a close path  $\gamma_B \in \mathfrak{S}([0, 1], \Omega)$ .

A complete edge-based active contour energy  $\mathcal{E}$  can be defined by the summation of an anisotropic edge-based term and a balloon term

$$\mathcal{E}(\gamma_B) = \int_0^1 \|\gamma'_B(v)\|_{\mathcal{M}_e(\gamma_B(v))} dv + \alpha E_{\text{balloon}}(\chi_B), \quad (6)$$

where  $\mathcal{M}_e : \Omega \rightarrow S_2^+$  is an edge-based tensor field and  $\alpha < 0$  is a constant.

Let  $\mathbf{g} \subset \Omega$  be a fixed shape and let  $U_{\mathbf{g}}$  be a tubular neighbourhood of a curve  $\gamma_{\mathbf{g}}$  such that  $U_{\mathbf{g}} := \{\mathbf{x} \in \Omega; \min_{v \in [0, 1]} \|\mathbf{x} - \gamma_{\mathbf{g}}(v)\| < r\}$  where  $r \in \mathbb{R}^+$  is a constant. Denoting by  $\mathbf{g}' = \mathbf{g} \setminus U_{\mathbf{g}}$  that is entirely determined by  $U_{\mathbf{g}}$ <sup>1</sup>. We define an admissible shape set  $\Phi(U_{\mathbf{g}}) := \{B \subset \Omega; \gamma_B \in \mathfrak{S}([0, 1], U_{\mathbf{g}}), \mathbf{g}' \subset B\}$ .

In the course of curve evolution, let  $\gamma_{B_k}$  ( $k > 0$ ) be the resulting curve in the  $k$ -th step. We note  $U_k$  as the tubular neighbour of  $\gamma_{B_k}$ . Our goal is to find an optimal curve  $\gamma_{B_{k+1}}$  such that  $B_{k+1} \in \Phi(U_k)$ . This can be done by solving

$$\inf_{A \in \Phi(U_k)} \mathcal{E}(\gamma_A) = \inf_{A \in \Phi(U_k)} \left\{ \int_0^1 \|\gamma'_A(v)\|_{\mathcal{M}_e(\gamma_A(v))} dv + \alpha \int_A d\mathbf{x} \right\}. \quad (7)$$

For any shape  $A \in \Phi(U_k)$ , one has the following equations

$$\begin{aligned} \mathcal{E}(\gamma_A) &= \int_0^1 \|\gamma'_A(v)\|_{\mathcal{M}_e(\gamma_A(v))} dv + \alpha \int_A d\mathbf{x} \\ &= \int_0^1 \|\gamma'_A(v)\|_{\mathcal{M}_e(\gamma_A(v))} dv + \alpha \int_A \chi_{U_k}(\mathbf{x}) d\mathbf{x} + C_{B_k}, \end{aligned} \quad (8)$$

where  $C_{B_k} = \alpha \int_{A \setminus U_k} d\mathbf{x}$  is a constant associated to the shape  $B_k$ . We consider a vector field  $\mathbf{a}_k$  that satisfies the following divergence equation

$$\text{div } \mathbf{a}_k = \alpha \chi_{U_k} \quad (9)$$

<sup>1</sup> This is because  $\mathbf{g}'$  is the bounded connected component of  $\Omega \setminus U_{\mathbf{g}}$ .

and suppose that  $\boldsymbol{\omega}_k(\mathbf{x}) = R \mathbf{a}_k(\mathbf{x})$ ,  $\forall \mathbf{x} \in \Omega$ , where  $R$  is the clockwise rotation matrix with angle  $\pi/2$ . We rewrite Eq. (8) by removing the constant  $C_{B_k}$

$$\begin{aligned} & \int_0^1 \|\gamma'_A(v)\|_{\mathcal{M}_e(\gamma_A(v))} dv + \alpha \int_A \chi_{U_k}(\mathbf{x}) d\mathbf{x} \\ &= \int_0^1 \|\gamma'_A(v)\|_{\mathcal{M}_e(\gamma_A(v))} dv + \int_0^1 \langle \mathbf{a}_k(\gamma_A(v)), \mathcal{N}(v) \rangle \|\gamma'_A(v)\| dv \end{aligned} \quad (10)$$

$$\begin{aligned} &= \int_0^1 \|\gamma'_A(v)\|_{\mathcal{M}_e(\gamma_A(v))} dv + \int_0^1 \langle \boldsymbol{\omega}_k(\gamma_A(v)), \mathcal{T}(v) \rangle \|\gamma'_A(v)\| dt \\ &= \int_0^1 \mathcal{F}_k(\gamma_A(v), \gamma'_A(v)) dv, \end{aligned} \quad (11)$$

where  $\mathcal{T} = R\mathcal{N}$  is the *clockwise* tangent of  $\gamma$  with the reality that  $\gamma' = \mathcal{T}\|\gamma'\|$ . The function  $\mathcal{F}_k$  is defined by

$$\mathcal{F}_k(\mathbf{x}, \mathbf{u}) = \|\mathbf{u}\|_{\mathcal{M}_e(\mathbf{x})} + \langle \boldsymbol{\omega}_k(\mathbf{x}), \mathbf{u} \rangle. \quad (12)$$

For a given shape  $B_k$ , the problem (7) is equivalent to

$$\inf_{A \in \Phi(U_k)} \int_0^1 \mathcal{F}_k(\gamma_A(v), \gamma'_A(v)) dv, \quad (13)$$

where the shape  $A$  is the interior region of the path  $\gamma_A$ . Note that the formulation (11) was first used in [10] for geodesic energy interpretation of a general region-based energy. Here we use it to convert the balloon force energy to a geodesic energy by a Finsler metric  $\mathcal{F}_k$ . The crucial point for the curve length energy (11) is the construction of the vector  $\boldsymbol{\omega}_k$  in Eq. (9). As discussed in [10], we solve the following PDE-constrained problem

$$\min \left\{ \int_{U_k} \|\boldsymbol{\omega}_k(\mathbf{x})\|^2 d\mathbf{x} \right\}, \quad s.t. \quad \operatorname{div} \boldsymbol{\omega}_k = \alpha \chi_{U_k}, \quad (14)$$

in an *optimization-then-discretization* manner to obtain the vector field  $\boldsymbol{\omega}_k$ .

**A new robust Finsler Metric.** The tensor field  $\mathcal{M}_e$  can be expressed by its eigenvalues  $\lambda_i$  and eigenvectors  $\boldsymbol{\nu}_i$  such that  $\mathcal{M}_e(\cdot) = \sum_i \lambda_i(\cdot) \boldsymbol{\nu}_i(\cdot) \boldsymbol{\nu}_i^T(\cdot)$  following that  $1 \leq \lambda_1(\cdot) \leq \lambda_2(\cdot)$ . The eigenvalues  $\lambda_i$  are computed according to the Frobenius norm of the gradient  $\nabla(G_\sigma * \mathbf{I})$  of a color image  $\mathbf{I}: \Omega \rightarrow \mathbb{R}^3$ , where  $\nabla(G_\sigma * \mathbf{I})$  is a *Jacobian matrix* with size  $2 \times 3$  and  $G_\sigma$  is a Gaussian filter with variance  $\sigma$ . Letting  $g$  be the Frobenius norm of the gradient  $\nabla(G_\sigma * \mathbf{I})$ , one has

$$\lambda_1(\cdot) = \exp(\beta_1 (\|g\|_\infty - g(\cdot))), \quad \lambda_2(\cdot) = \exp(\beta_2 g(\cdot)) \lambda_1(\cdot),$$

where  $\beta_1$  and  $\beta_2$  are two positive constants. The vector  $\boldsymbol{\nu}_1(\cdot)$  is the eigenvector of  $\nabla(G_\sigma * \mathbf{I})(\cdot)$  corresponding to the smaller eigenvalue. Thus  $\boldsymbol{\nu}_1(\mathbf{x})$  is collinear to the edge orientation at  $\mathbf{x}$ . The vector  $\boldsymbol{\nu}_2(\cdot)$  is the remaining eigenvector of  $\nabla(G_\sigma * \mathbf{I})(\cdot)$ . In this case,  $\beta_2$  controls the anisotropy of the tensor field  $\mathcal{M}_e$ . If  $\mathbf{x}$  is far from the boundaries, one has  $\lambda_1(\mathbf{x}) \approx \lambda_2(\mathbf{x}) \gg 1$ , leading to an

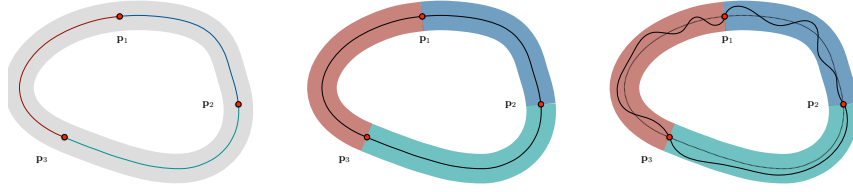


**Fig. 1.** Illustration for the procedure of interactive image segmentation. **Column 1** Control points  $\mathbf{p}_i$  (red dots) and tubular neighbourhood (gray region). **Column 2** Separated tubular subregions. **Column 3** Extracted minimal paths (solid black curves) between successive control points.



**Fig. 2.** Evolution course of the interactive image segmentation scheme. **Column 1** Initialization. Red dots are the control points. **Columns 2-5** Segmentation results from the first iteration to the fourth iteration.

approximately isotropic tensor  $\mathcal{M}_e(\mathbf{x})$  and high metric cost at  $\mathbf{x}$ . In contrast, if  $\mathbf{x}$  is near a boundary, one has  $\lambda_2(\mathbf{x}) \gg 1$  and  $\lambda_1(\mathbf{x}) \approx 1$  corresponding to an highly anisotropic tensor  $\mathcal{M}_e(\mathbf{x})$ .

To obey the positive constraint (4), we should ensure that  $\inf_{\mathbf{x}} \|\omega_k(\mathbf{x})\| < 1$ . We make use of a non-linear map to construct a new vector field  $\tilde{\omega}$  such that

$$\tilde{\omega}_k(\mathbf{x}) = (1 - \exp(-\tilde{\alpha} \|\omega_k(\mathbf{x})\|)) \omega_k(\mathbf{x}) / \|\omega_k(\mathbf{x})\|, \quad (15)$$

where  $\tilde{\alpha}$  is a positive parameter. The Finsler metric  $\mathcal{F}_k$  in Eq. (12) thus becomes

$$\tilde{\mathcal{F}}_k(\cdot, \mathbf{u}) = \|\mathbf{u}\|_{\mathcal{M}_e(\cdot)} + \langle \tilde{\omega}(\cdot), \mathbf{u} \rangle. \quad (16)$$

Since the balloon force is only used to drive the curves outward, the use of the reconstructed Finsler metric  $\tilde{\mathcal{F}}$  will not modify the goal that  $\mathcal{F}$  services for [10].

**Interactive Segmentation.** A curve concatenation operator can be defined by

$$\Gamma(v) = (\Gamma_1 \uplus \Gamma_2)(v) = \begin{cases} \Gamma_1(2v), & \text{if } 0 \leq v < \frac{1}{2}, \\ \Gamma_2(2v - 1), & \text{if } \frac{1}{2} \leq v < 1, \end{cases}$$

where  $\Gamma, \Gamma_1, \Gamma_2 \in \mathfrak{S}([0, 1], \Omega)$  are clockwise paths.

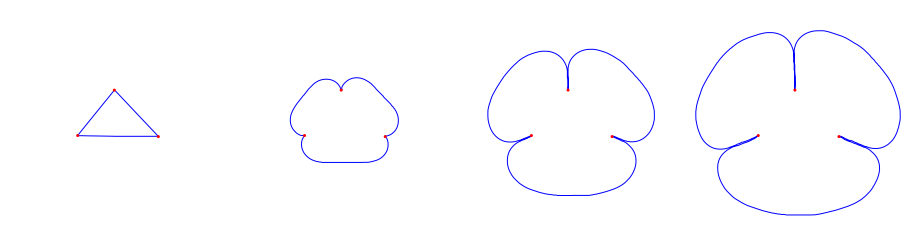


**Fig. 3.** Curve evolution with  $\mathcal{M}_e \equiv \mathbf{I}_d$ . **Column 1** Control points and initial contour. **Columns 2-3** Evolution results on different iterations.

Considering a collection  $\{\mathbf{p}_i\}_{i \leq m}$  of  $m$  ( $m \geq 3$ ) user-provided control points distributed in a *clockwise* order along an object boundary. We aim to search for a closed contour to delineate the target object boundary. This can be done by concatenating a set of minimal paths associated to the metric  $\mathcal{F}_k$ , each of which links a pair of successive landmark points  $\{\mathbf{p}_i, \mathbf{p}_{i+1}\}$ . In Fig. 1a, we show three control points denoted by red dots. During the curve evolution, in the  $k$ -th iteration, we denote by  $\mathcal{C}_{i,k}$  the paths between each pair of successive control points  $\mathbf{p}_i$  and  $\mathbf{p}_{i+1}$  for  $i < m$ , and by  $\mathcal{C}_{m,k}$  the path linking  $\mathbf{p}_m$  to  $\mathbf{p}_1$ . A closed contour  $\gamma_{B_k}$ , indicating the exterior boundary of the shape  $B_k$ , can be concatenated by  $\gamma_{B_k} = \uplus_{i=1}^m \mathcal{C}_{i,k}$ . Let  $U_k$  be the tubular neighbourhood of  $\gamma_{B_k}$ . One can identify a subregion  $\mathfrak{R}_i \subset U_k$  for each path  $\mathcal{C}_{i,k}$

$$\mathfrak{R}_i := \{\mathbf{x} \in U; d(\mathbf{x}, \mathcal{C}_{i,k}) < d(\mathbf{x}, \mathcal{C}_{j,k}), \forall j \neq i\} \cup \{\mathcal{C}_{i,k}(0), \mathcal{C}_{i,k}(1)\}.$$

In Fig. 1b, we illustrated each subregion  $\mathfrak{R}_i$  by different colours.

Within each region  $\mathfrak{R}_i$ , we take  $\mathbf{p}_i$  as the source point to compute the geodesic distance map  $\mathcal{U}_{\mathbf{p}_i}$  with respect to the metric  $\mathcal{F}$  via the solution to the Eikonal PDE (1). Then a minimal path  $\mathcal{C}_{i,k+1}$  is obtained by using  $\mathcal{U}_{\mathbf{p}_i}$  and the gradient descent ODE (2). The desired closed contour  $\gamma_{B_{k+1}}$  can be concatenated by

$$\gamma_{B_{k+1}} = \uplus_{i=1}^m \mathcal{C}_{i,k+1}, \quad (17)$$

and the shape  $B_{k+1}$  can be simply identified as the interior region of  $\gamma_{B_{k+1}}$ . Once we obtain  $\gamma_{B_{k+1}}$ , the vector field  $\tilde{\omega}_{k+1}$  and metrics  $\tilde{\mathcal{F}}_{k+1}$  can be updated using Eqs. (15) and (16), respectively. We illustrate the course of the interactive segmentation in Fig. 2, where the proposed model can converge to the desired object boundary in only 4 steps. The curve evolution can be terminated when the Hausdorff distance between two curves  $\gamma_{B_k}$  and  $\gamma_{B_{k+1}}$  is small enough.

**Remark.** The path  $\mathcal{C}_{i,k}$  is actually a globally minimizing curve in the domain  $\mathfrak{R}_i$  with respect to the Finsler metric  $\tilde{\mathcal{F}}_k$ , which leads the proposed method to be insensitive to spurious edges and noise. Moreover, the definition of  $\mathfrak{R}_i$  guarantees the extracted closed contour  $\gamma_{B_{k+1}}$  (see Eq. (17)) to be a simple curve since each pair of subregions  $\mathfrak{R}_i$  and  $\mathfrak{R}_j$  has only one intersection point.

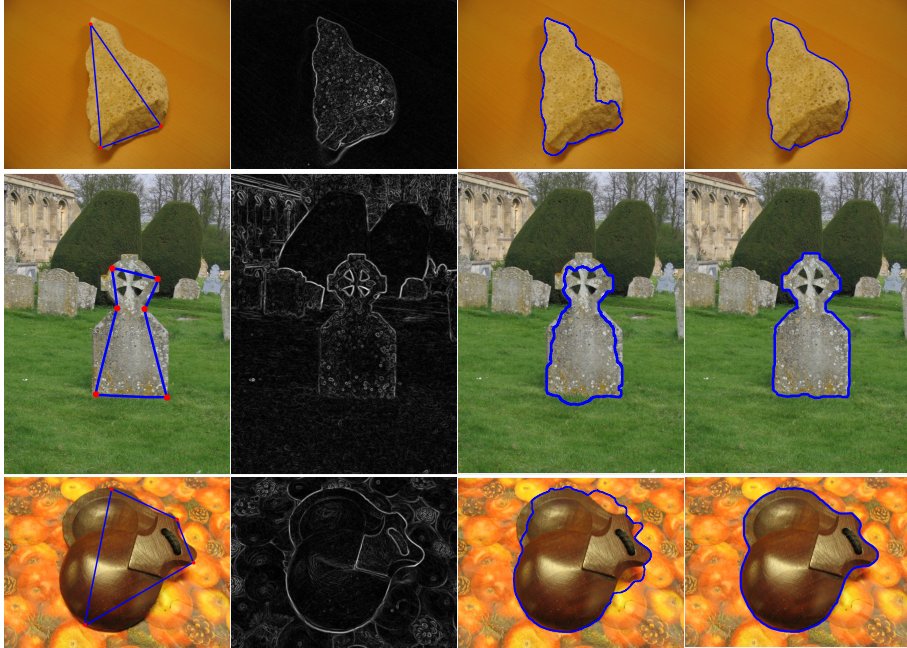


**Fig. 4.** Image segmentation results. **Column 1** Initializations. Red dots are user-specified control points. **Column 2** Edge saliency map. **Column 3** Segmentation from GAC model. **Column 4** Segmentation from the proposed model.

## 4 Experimental Results

In Fig. 3, we show the curve evolution results by setting the tensor field  $\mathcal{M}_e \equiv \mathcal{I}_d$ , where  $\mathcal{I}_d$  is the identity matrix. These contours (blue curves) inflate outward in the course of the curve evolution due to the balloon force (negative value of  $\alpha$ ). In this experiment the control points  $\mathbf{p}_i$  (red dots) have been fixed. Moreover, as an option, these control points can be resampled in each iteration (for details we refer to [10]). In this case, the contours (blue curves) will tend to appear as a circle and will expand indefinitely since there is no edges to stop the evolution.

We compare our method to the GAC model [2]. The gradient flow of the GAC model with respect to a level set function<sup>2</sup>  $\psi$  can be expressed by

$$\psi_t = \|\nabla\psi\| \operatorname{div}(f \nabla\psi / \|\nabla\psi\|) + c f \|\nabla\psi\|, \quad (18)$$

where  $f(\cdot) = \exp(-\beta_2 g(\cdot))$  and  $g$  is defined as the Frobenius norm of the gradient  $\nabla(G_\sigma * \mathbf{I})$ . The term  $c f \|\nabla\psi\|$  with  $c < 0$  services as the adaptive balloon force such that the curves will go outward in the flatten region where the edge indicator  $f(\cdot) \gg 0$ . In columns 3 and 4 of Fig. 4, we show the comparison results of the GAC model and our method, where the corresponding initializations are

<sup>2</sup> We use the distance preserving method [18] to avoid level set reinitialization.

illustrated in column 1. We also show the edge saliency map in column 2. One can see that the proposed model can successfully catch the desired boundaries. In each tubular subregions  $\mathfrak{R}_i$ , our method can find the robust and globally (w.r.t  $\mathfrak{R}_i$ ) minimizing curve. In the column 3 of the GAC results, some portions of the contours leak outside the boundaries due to the constant  $c$  for the adaptive balloon force in Eq. (18). At the same time, some parts of the contours fall into unexpected local minimums that are inside the objects. We can claim that compared to the GAC model, the main advantages of the proposed method are the robust optimality and the use of the user-specified control points.

## 5 Conclusion

In this paper, we propose a new edge-based active contour model based on the Finsler Eikonal PDE. The basic idea is to convert the balloon regional term as a curve energy via an asymmetric Finsler metric including the anisotropic edge information. The proposed model is able to blend the benefits from the global optimality of minimal path framework, the efficiency of the fast marching method and the user intervention. Experiments show that our model indeed obtains promising results.

## References

1. Kass, M., Witkin, A., Terzopoulos, D.: Snakes: Active contour models. *IJCV* **1**(4) (1988) 321–331
2. Caselles, V., Kimmel, R., Sapiro, G.: Geodesic active contours. *IJCV* **22**(1) (1997) 61–79
3. Yezzi, A., Kichenassamy, S., Kumar, A., Olver, P., Tannenbaum, A.: A geometric snake model for segmentation of medical imagery. *TMI* **16**(2) (1997) 199–209
4. Melonakos, J., Pichon, E., Angenent, S., Tannenbaum, A.: Finsler active contours. *TPAMI* **30**(3) (2008) 412–423
5. Jbabdi, S., Bellec, P., et al.: Accurate anisotropic fast marching for diffusion-based geodesic tractography. *JBFI* **2008** (2008) 2
6. Osher, S., Sethian, J.A.: Fronts propagating with curvature-dependent speed: algorithms based on Hamilton-Jacobi formulations. *JCP* **79**(1) (1988) 12–49
7. Cohen, L.D., Kimmel, R.: Global minimum for active contour models: A minimal path approach. *IJCV* **24**(1) (1997) 57–78
8. Appia, V., Yezzi, A.: Active geodesics: Region-based active contour segmentation with a global edge-based constraint. In: *Proceedings of ICCV’11*. (2011) 1975–1980
9. Mille, J., Bougleux, S., Cohen, L.: Combination of piecewise-geodesic paths for interactive segmentation. *IJCV* **112**(1) (2014) 1–22
10. Chen, D., Mirebeau, J.M., Cohen, L.D.: Finsler geodesic evolution model for region-based active contours. In: *Proceedings of BMVC’16*. (2016)
11. Cohen, L.D.: On active contour models and balloons. *CVGIP: Image Understanding* **53**(2) (1991) 211–218
12. Chen, D., Mirebeau, J.M., Cohen, L.D.: Global minimum for a Finsler elastica minimal path approach. *IJCV* **122**(3) (2017) 458–483

13. Mirebeau, J.M.: Efficient fast marching with Finsler metrics. *Numerische Mathematik* **126**(3) (2014) 515–557
14. Sethian, J.A., Vladimirsky, A.: Ordered upwind methods for static Hamilton–Jacobi equations: Theory and algorithms. *SINUM* **41**(1) (2003) 325–363
15. Chen, D., Cohen, L.D.: Fast asymmetric fronts propagation for image segmentation. Preprint (2017)
16. Randers, G.: On an asymmetrical metric in the four-space of general relativity. *Physical Review* **59**(2) (1941) 195
17. Chan, T.F., Vese, L.A.: Active contours without edges. *TIP* **10**(2) (2001) 266–277
18. Li, C., Xu, C., et al.: Distance regularized level set evolution and its application to image segmentation. *TIP* **19**(12) (2010) 3243–3254